Thin Films of Homopolymers and Cylinder-Forming Diblock Copolymers under Shear

Arash Nikoubashman,[†] Raleigh L. Davis,[†] Brian T. Michal,[†,§] Paul M. Chaikin,[‡] Richard A. Register,[†] and Athanassios Z. Panagiotopoulos[†,*]

[†]Department of Chemical and Biological Engineering, Princeton University, Princeton, New Jersey 08544, United States, and [‡]Center for Soft Matter Research and Department of Physics, New York University, New York, New York 10003, United States. [§]Present address: Department of Macromolecular Science and Engineering, Case Western Reserve University, Cleveland, Ohio 44106, United States.

ABSTRACT We study thin films of homopolymers (PS) and monolayers of cylinder-forming diblock copolymers (PS—PHMA) under shear. To this end, we employed both experiments and computer simulations that correctly take into account hydrodynamic interactions and chain entanglements. Excellent quantitative agreement for static as well as dynamic properties in both the homopolymer and diblock copolymer cases was achieved. In particular, we found that the homopolymer thin films exhibit a distinct shear thinning behavior, which is strongly correlated with the disentanglement and shear alignment of the constituent polymer chains. For the PS—PHMA films, we show that shear can be employed to induce long-range ordering to the spontaneously self-assembled microdomains, which is required for many applications such as the fabrication of nanowire arrays. We found that the impact of chemical incompatibility on the viscosity is only minor in shear-aligned films. Once the domains were aligned, the films exhibited an almost Newtonian response to shear because the cylindrical microdomains acted as guide rails, along which the constituent copolymer chains could simply slide. Furthermore, we developed a model for predicting the onset of shear alignment based on equilibrium dynamics data, and found good agreement with our shear simulations. The employed computational method holds promise for a faster and more cost-effective route for developing custom tailored materials.

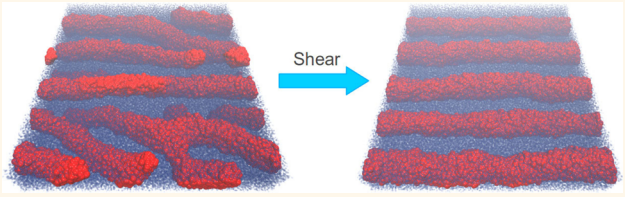

KEYWORDS: thin films · homopolymers · cylinder-forming diblock copolymers · shear

Soft materials have gained increasing interest in science and technology, due to their inherent capacity to self-assemble into well-ordered structures on the nanoscale, which is a key requirement for the fabrication of nanolithography masks and the miniaturization of electronic devices.[1−3] Furthermore, self-assembly is typically low-cost, fast, and easily scalable, which makes it attractive for large-scale industrial applications. Promising candidates are block copolymers, which are macromolecules that consist of two (or more) chemically distinct blocks covalently bonded to each other. These polymers self-assemble into nanoscale domains when the constituent blocks are immiscible and the melt is below the order−disorder temperature. Depending on the composition, morphologies such as lamellae, gyroid, cylinders, and spheres can be produced.[4] However, spontaneously formed structures typically lack long-range order, which is required when using block copolymer thin films in nanopatterning applications, for instance, the fabrication of nanowire grids for deep UV polarizers.[5−8] Macroscopic alignment can be induced through the application of steady shear, which has been shown to orient the microdomains in the direction of applied shear.[9,10] Shear alignment has several advantages over alternative strategies, *e.g.*, surface patterning,[2] electric fields,[11−13] and thermal gradients,[14−16] including applicability over an arbitrary range of polymer chemistries and morphologies,[9,17,18] no need for doping or exotic material properties, no prepatterning of the substrate required, and the ability to align microdomains over macroscopic length scales. All of these features make this process amenable to large-scale industrial manufacturing using roller printing techniques.[19,20]

In order to reliably fabricate aligned films with low defect densities on macroscopic

* Address correspondence to azp@princeton.edu.

Received for review April 14, 2014 and accepted August 8, 2014.

Published online August 08, 2014
10.1021/nn502068e

scales through shear, knowledge about the rheological properties of these materials is crucial. Determining these quantities *via* experiments typically involves a series of intricate steps, such as synthesizing the copolymers, preparing the thin films, and finally executing the shear alignment procedure. However, such conventional prototyping is often prohibitively costly and time-consuming, and therefore alternative approaches are desirable. One viable option is computer simulations, which potentially allow for significantly shorter turnaround times and microscopic insights into the system. Indeed, simulations have significantly contributed to better understanding the static and dynamic properties of polymer melts.[21−25] Here, particular attention has been devoted to the study of polystyrene (PS), one of the most common thermoplastic polymers encountered in everyday life.[24] Several atomistic and coarse-grained (CG) bead−spring models have been developed for PS,[26,27] which faithfully reproduce the microscopic characteristics of the experimental system. However, these models are unfeasible for most practical situations, since they are rather computationally intensive, and therefore only allow for the sampling of relatively small systems and short time scales. These system size issues become even more problematic for the study of block copolymers under shear, since the long-range ordering of the microdomains is of central interest in these cases. On the other hand, mean-field methods such as cell dynamics[23] and self-consistent field theory[28] enable simulations over long time scales and for large system sizes, but prohibit the analysis of microscopic properties. Furthermore, these overly simplified models often reproduce only qualitative trends,[29] thereby limiting their practical use for describing specific systems and predicting material properties. This is especially true for the rheological properties, due to the inherent accelerated dynamics of such heavily coarse-grained models.[24,25]

We address these long-standing issues by employing a more sophisticated CG model that correctly takes into account both hydrodynamic interactions and chain entanglements, thus reproducing the correct reptation dynamics. In order to demonstrate the general feasibility of our approach, we first conducted simulations of a PS homopolymer melt under shear and achieved excellent quantitative agreement with literature data. We then extended our studies to monolayer films of cylinder-forming diblock copolymers under steady shear. To this end, we performed both experiments and computer simulations and observed the shear-induced long-range ordering of the cylindrical microdomains with a concomitant shear-thinning. The predicted shear viscosity from our simulations was two times higher than the value measured in our experiments, and we provide a discussion on the origin of this discrepancy. Finally, we established a theoretical framework for estimating the onset of shear alignment from equilibrium dynamic data.

RESULTS AND DISCUSSION

We employed the so-called theoretically informed coarse graining (TICG) approach[30] in conjunction with the dissipative particle dynamics (DPD) simulation method[31−34] for modeling the polymer melts. This bead−spring model captures the essential properties of the experimental systems, and has recently been successfully employed for describing various diblock copolymer systems in and out of equilibrium.[30,35−38] In this strongly coarse-grained model, the interaction sites are ultrasoft beads allowing for full and multiple particle overlaps and bond-crossing. Although this deficiency does not pose any problem for the investigation of static properties, it needs to be addressed for dynamic simulations since the absence of these topological constraints leads to accelerated dynamics and may cause an unrealistic rheology of the system. Therefore, we reintroduce entanglement effects into the system through slip-springs, which recover the correct reptation dynamics in the melt.[37,39] For a more detailed discussion of the model and simulation method, we refer the reader to the Methods section of the manuscript and the Supporting Information (SI).

Homopolymers. In order to verify the general feasibility of our theoretical approach and to establish a baseline for the poly(styrene)-*b*-poly(*n*-hexyl methacrylate) (PS−PHMA) diblock copolymer systems, we initially studied a polystyrene homopolymer melt and computed its dynamic properties; PS is a convenient choice as experimental data are broadly available for this polymer. In particular, we modeled linear PS chains with a molecular weight of $M = 75$ kg/mol at $T = 458$ K, which is well above its glass transition temperature ($T_g = 376$ K). M exceeds the critical molecular weight of PS ($M_c \approx 31$ kg/mol), which indicates the transition from the Rouse to the reptation regime, and therefore entanglement effects need to be considered (see Materials).[40,41]

Coarse-grained simulations are known to produce accelerated dynamics when the intrinsic time scale ($\tau \sim a(m/\varepsilon)^{1/2}$, see Methods) is used as a measure of time. In order to make meaningful predictions for specific systems, it is crucial to establish a connection between the time-scale of our simulations, τ, and experiments.[24] We achieved this by matching the long-time diffusion coefficient D_0 of experiments in the bulk with simulations using periodic boundary conditions. Figure 1 shows the mean square displacement $\Delta r^2(t) = |\mathbf{r}(t') - \mathbf{r}(t' + t)|^2$ of the polymer's central bead, and we can identify three distinct regions: for $t/\tau \ll 1$, we found $\Delta r^2(t) \propto t^2$ reflecting the ballistic motion of the constituent monomers at short time scales. In the intermediate regime $5 \lesssim t/\tau \lesssim 250$ we observed a strongly subdiffusive behavior with $\Delta r^2(t) \propto t^{0.37}$. The measured

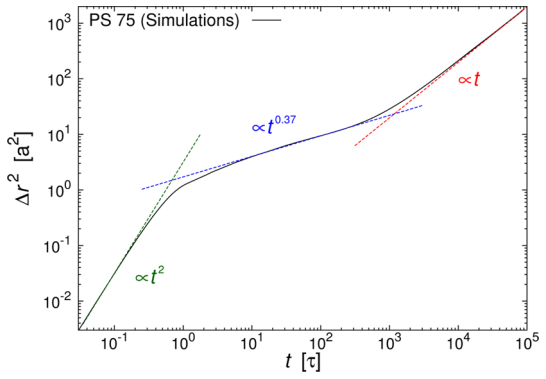

Figure 1. Mean square displacement $\Delta r^2(t)$ of a polystyrene homopolymer with M = 75 kg/mol in the melt at T = 458 K from simulations. The dashed lines are fits to our data and indicate the different diffusion regimes.

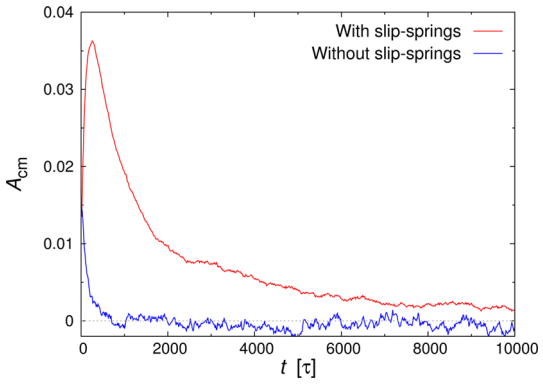

Figure 2. Correlation between the motion of the center of mass $\mathbf{r}_{cm}$ and the end-to-end vector $\mathbf{r}_e$ of a PS 75 chain calculated from simulations.

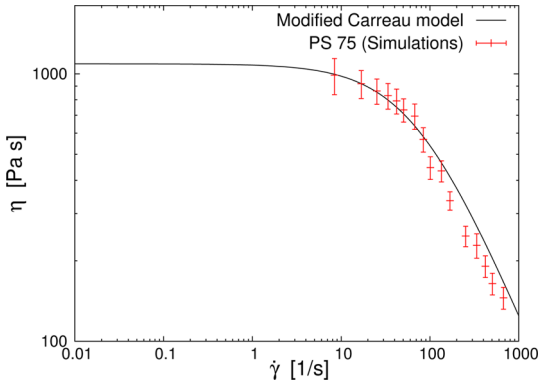

Figure 3. Shear viscosity $\eta(\dot{\gamma})$ of a melt of linear PS chains with M = 75 kg/mol at T = 458 K. The continuous line depicts the prediction of the modified Carreau model (see eq 3 and ref 45), while the symbols show the simulation results.

exponent lies between the expected values for Rouse dynamics (1/2) and reptation dynamics (1/4),[37,39] and reflects the weak but still existent entanglement of the chains. Finally, normal diffusion is recovered for $t/\tau \gtrsim 10^4$. Here, we obtained $D_0 = 0.0034\ a^2/\tau$ through the relation $6D_0t = \Delta r^2(t)$, while ref 42 reports a value of $D_0 = 0.55 \times 10^{-11}$ cm^2/s for the corresponding experimental system. In conjunction with the length-scale a = 3.2 nm (see Methods), these data lead to the time scale τ = 63 μs.

To better understand the effect of reptation in the melt, we calculated the correlation between the motion of the center of mass $\mathbf{r}_{cm}$ and the end-to-end vector $\mathbf{r}_e$ of the chain through[43]

$$A_{cm}(t) = \frac{3}{2}\left[\left\langle\left(\frac{\mathbf{a}(t)\cdot\mathbf{b}(t)}{|\mathbf{a}(t)||\mathbf{b}(t)|}\right)^2\right\rangle - \frac{1}{3}\right] \qquad (1)$$

with $\mathbf{a}(t) = \mathbf{r}_{cm}(t) - \mathbf{r}_{cm}(0)$ and $\mathbf{b}(t) = [\mathbf{r}_e(t) + \mathbf{r}_e(0)]/2$. In general, this definition ensures that only a motion parallel to the vector $\mathbf{b}(t)$ results in $A_{cm}(t) = 1$, while an isotropic motion yields $A_{cm}(t) = 0$. For unentangled polymers, $A_{cm}(t)$ quickly decays to zero, whereas entangled polymers are confined in a tube-like environment and therefore exhibit an anisotropic motion predominantly parallel to their contour. This difference is clearly visible in Figure 2, where we have plotted $A_{cm}(t)$ for a PS 75 chain in the melt with and without slip-springs. The initial nonzero value of $A_{cm}(0)$ is due to excluded volume interactions, which are identical in both cases. In the simulations with slip-springs, A_{cm} increases until it reaches its maximum at $t/\tau \approx 250$, and then slowly decays to 0. These transitions are consistent with our measurements of the mean square displacement $\Delta r^2(t)$.

Another important dynamic property of a polymeric melt is the viscosity η, which quantifies its resistance to gradual deformation under shear stress. The zero-shear viscosity of the PS melt was measured experimentally[44] as η_0 = 1090 Pa·s using a cone-and-plate rheometer at a shear rate of $\dot{\gamma} = 2.7 \times 10^{-4}$ s^{-1}, which is well below the onset of shear-thinning.[45] In the simulations, we calculated η_0 for a bulk system of PS 75 *via* the Green−Kubo relation:

$$\eta_0 = \frac{V}{k_B T}\int_0^\infty \langle P_{\alpha\beta}(0)P_{\alpha\beta}(t)\rangle\, dt \qquad (2)$$

where $P_{\alpha\beta}$ denote the off-diagonal components of the pressure tensor. Here, we found a value of η_0 = 1140 Pa·s (±10%), which is in very good agreement with the experimental results. Next, we studied the shear rate dependence of the viscosity, $\eta(\dot{\gamma})$. Here, it is well-known that polymer melts exhibit a strong shear-thinning behavior at sufficiently high shear rates, due to the alignment of the individual polymer chains along the flow direction. This non-Newtonian behavior can be well described for PS through the modified Carreau model:[46−48]

$$\eta(\dot{\gamma}) = \frac{\eta_0}{[1 + (\eta_0\dot{\gamma}/k^*)]^{(1-n)}} \qquad (3)$$

where the parameters k^* and n control the onset and the amount of shear thinning, respectively. These two parameters have been determined in ref 45 for PS melts with low dispersities ($1.0 \leq Đ \leq 1.1$) under steady shear as $k^* = 7.67 \times 10^4$ Pa and n = 0.203. Figure 3

shows the resulting $\eta(\dot{\gamma})$ for the model PS chains investigated here, illustrating the Newtonian and power-law asymptotes found at low and high $\dot{\gamma}$, respectively.

In the simulations, we have determined $\eta(\dot{\gamma})$ by shearing a thin film of PS with a constant shear rate $\dot{\gamma}$ and computed the shear stress σ_{zx} necessary to maintain steady shear conditions (see SI for details). Here, we chose a film thickness of $H = 60$ nm $\approx 8\ R_{g,0}$ (with equilibrium radius of gyration $R_{g,0}$), and carefully checked for finite-size effects by conducting additional simulations at $H = 120$ nm for selected $\dot{\gamma}$. No such effects were observed, and hence we expect the same response to shear as in the bulk. We imposed no-slip boundary conditions at the immediate wall-film interfaces (see Methods), which is analogous to the procedure in experiments, where shear is only applied at the film surfaces and the velocity profile across the film builds up self-consistently. Alternative simulation methods, where a linear velocity profile is superimposed, are unphysical, as they mask the system's response to shear. Once the system reached a steady state, we computed $v_x(z)$, *i.e.*, the velocity profile along the gradient direction, and found a sizable slip across the film, which is due to the high viscosity of the polymer melt. Hence, the effective shear rate transmitted by the walls to the interior of the confined film is lower than that implied by the applied shear at the walls. For this reason, we measured the velocity profiles in the middle of the film ($-H/4 < z < +H/4$) and calculated the effective shear rate, $\dot{\gamma}_{\text{eff}}$, for determining $\eta(\dot{\gamma})$. Figure 4 shows the emerging velocity profiles $v_x(z)$ for selected $\dot{\gamma}$, and it is visible that $\dot{\gamma}_{\text{eff}}$ approaches $\dot{\gamma}$ with increasing shear rate.

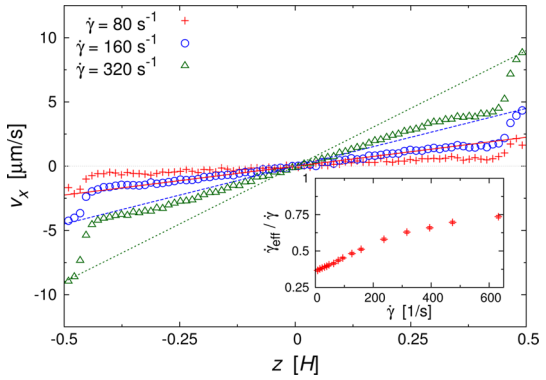

Figure 4. Velocity profiles along the gradient direction $v_x(z)$ for a PS polymer melt under steady shear at $\dot{\gamma} = 80$, 160, and 320 s^{-1}. The lines indicate the theoretical velocity profiles for a Newtonian fluid, while symbols show the actual velocity profile from simulations. Inset: ratio $\dot{\gamma}_{\text{eff}}/\dot{\gamma}$ as a function of applied shear rate $\dot{\gamma}$.

As shown in Figure 3, the simulations correctly replicate the shear-thinning behavior found at high $\dot{\gamma}$ and perfectly coincide with the experimental findings. Furthermore, we can use these data to check the self-consistency of our measurements by determining the zero-shear viscosity η_0 from our shear simulations and compare it to the result under quiescent conditions. To this end, we fit our data through eq 3, where we set k^* and n to the experimental values for bulk PS and kept η_0 as a free parameter. This procedure led to $\eta_0 =$ 1090 Pa·s (±3%), which is in excellent quantitative agreement with both the experimental value for bulk PS and our calculations using the Green−Kubo formalism. In contrast, simulations without slip-springs resulted in viscosities lower by a factor of ∼2 and an exaggerated shear-thinning behavior.

To understand better the origin of the shear-thinning, we studied the conformation of the sheared polymers. First, we investigated the diagonal components of the gyration tensor $R_{\alpha\alpha}$ as a function of $\dot{\gamma}$. The results are shown in Figure 5(a), and it is clear that the polymers are (almost) fully isotropic at rest, but then quickly elongate along the flow direction (x) as shear is applied. At the same time, the polymers slightly contract along the gradient (z) and vorticity direction (y) of the shear flow, with $R_{zz} < R_{yy}$ throughout due to the presence of the walls in the xy-plane. In order to exclude any unphysical simulation artifacts, we also

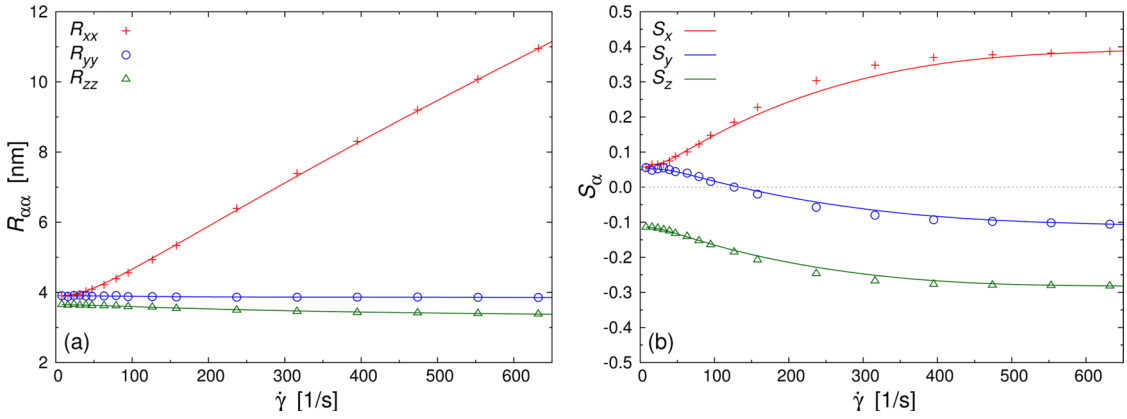

Figure 5. Diagonal components of the gyration tensor $R_{\alpha\alpha}$, (a), and the second Legendre polynomial S_α, (b), of the PS homopolymers along the flow (x), vorticity (y), and gradient direction (z) of the shear flow. The solid lines are guides to the eye.

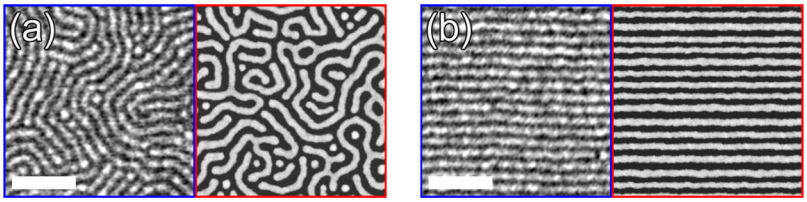

Figure 6. Film morphologies before (a) and after applying shear (b). The left half of each image shows experimental results obtained by TM-AFM, while the right half shows typical simulation snapshots. The scale bars indicate 200 nm.

computed the bond stretching due to the applied flow, and found that the stretching was below 2% for the highest flow strengths applied.

Next, we quantified the alignment of the polymer chains *via* the second Legendre Polynomial S_α, also known as the Hermans orientation function, which is defined as follows:

$$S_\alpha = \frac{1}{2}[3\cos^2\theta_\alpha - 1] \quad (4)$$

where θ_α is the angle between the end-to-end vector of the polymer and the Cartesian axes $\alpha \in \{x,y,z\}$. The order parameter S_α has an upper bound at 1, which corresponds to full alignment along the α-axis, and a lower bound at −0.5, which represents configurations in the plane perpendicular to the α-axis. $S_\alpha = 0$ indicates that the chains do not have any preferred orientation in that specific direction. The simulation results for the PS homopolymer melt are shown in Figure 5(b): under quiescent conditions, the polymers are slightly aligned in the *xy*-plane due to the presence of the walls along the *z*-direction. As the thin film was sheared, the polymers aligned in the flow direction, while losing their weak ordering in the vorticity direction. Furthermore, it is apparent that the upper bound of 1 is not reached for the investigated $\dot{\gamma}$ values, because of thermal fluctuations and entanglements between the polymer chains.

By comparing Figure 3 with Figure 5(a,b) it becomes clear that the onset of shear-thinning at $\dot{\gamma}_c \approx 10\ s^{-1}$ is directly related to the gradual alignment of the individual polymer chains. Theoretical considerations based on the Rouse model predict that the longest relaxation time of the polymers follows the relation $\tau_1 = R^2_{g,0}/D_0$.[40,49] We can then define the onset $\dot{\gamma}$ for shear-thinning as $\dot{\gamma}_c = \tau_1^{-1}$, which leads to a value of $\dot{\gamma}_c \approx 10\ s^{-1}$ for the investigated PS homopolymer melt. This estimation is in excellent agreement with our simulation results (*cf.* Figure 3), thereby verifying the integrity of our model and simulation method.

Diblock Copolymers. We then studied the dynamic properties of a thin film of cylinder-forming diblock copolymers, where we chose PS−PHMA as our model system (see Materials for more detailed information). These systems differ fundamentally from the previously investigated homopolymer melts, since they segregate into PS- and PHMA-rich microdomains due to the chemical incompatibility of the constituent blocks. PS−PHMA possesses several properties that make it particularly useful for pattern transfer. During reactive ion etching with CF_4, PHMA etches at more than twice the rate of PS; the etch contrast can be further enhanced through RuO_4 staining of the PS.[6,7] This etch rate contrast enables pattern transfer *via* etching into the underlying substrate. Another practical advantage of PS−PHMA is the ease with which it can be imaged *via* atomic force microscopy (AFM). At room temperature, the glassy PS cylinders (T_g = 376 K) and the rubbery PHMA matrix (T_g = 268 K)[50] possess a substantial viscoelastic mismatch which creates a strong phase contrast when operating the AFM in tapping mode (TM-AFM). This makes imaging the thin film morphology and assessing the alignment quality after shear simple and accurate, with no need to enhance/create contrast *via* etching or solvent swelling, which could distort the imparted alignment. Finally, styrene and *n*-hexyl methacrylate are abundant monomers whose living anionic polymerization has been well studied, enabling the production of PS−PHMAs of narrow dispersity and controlled molecular weight, composition, and microdomain size and spacing.

After the PS−PHMA monolayers spontaneously microphase-separated [see Figure 6(a)], we induced long-range order through steady shear. In the simulations, this was done analogously to the PS case discussed above. In the experiments, we applied a constant shear stress σ_{zx} to the samples through pad shearing and then calculated the apparent shear rate $\dot{\gamma}$ through the displacement of the pad (see Methods). We focused on monolayer films of PS−PHMA (H = 28 nm), where the copolymers spontaneously self-assembled into cylinders parallel to the film interface.[36] Such initial configurations are preferable for achieving good alignment quality postshear (*i.e.*, fewest dislocations, and smallest angular spread of cylinder orientations), since the majority of microdomains are already oriented in the shear plane and thus fewer realignments are necessary during the shearing.[9] Figure 6 shows both an experimental phase image obtained through TM-AFM and a simulation snapshot of a PS−PHMA monolayer before and after shear was applied. This comparison highlights the effect of steady shear on the long-range ordering as well as the good agreement between our experiments and simulations.

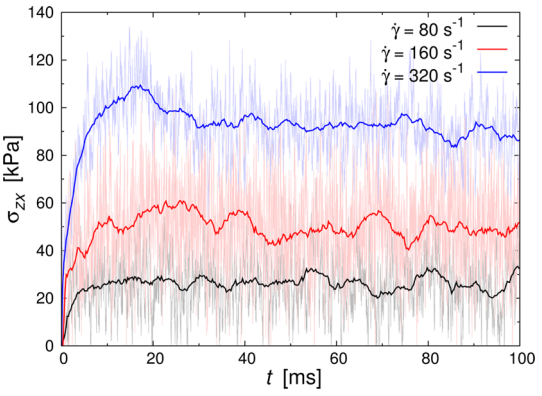

Figure 7. Shear stress σ_{zx} as a function of time t for a monolayer of cylinder-forming PS−PHMA 24/89 at various shear rates $\dot{\gamma}$ from our simulations. Light colored lines correspond to the instantaneous value of σ_{zx}, while the dark lines are running averages with a sampling window of 0.2 ms.

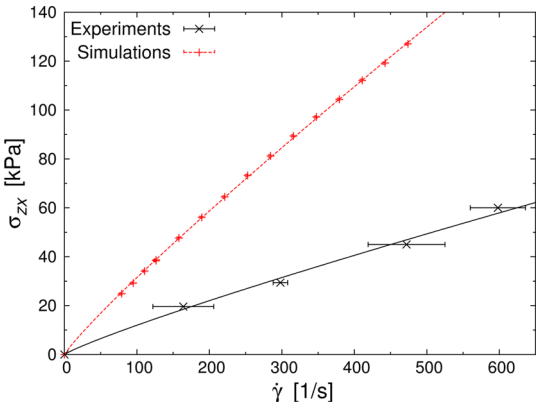

Figure 8. Shear stress σ_{zx} as a function of shear rate $\dot{\gamma}$ for a monolayer of cylinder-forming PS−PHMA 24/89 from experiments (black) and simulations (red).

Figure 7 shows the temporal evolution of the shear stress σ_{zx} for an initially unaligned monolayer of PS−PHMA 24/89 during the startup of shear, obtained by simulations. Here, it is apparent that the computed σ_{zx} slowly increases as the shear is turned on until it converges to its steady state value. Furthermore, we can identify a slight overshoot of σ_{zx} at sufficiently high $\dot{\gamma}$, which is typical for entangled polymer solutions and melts.[37,51−55] This overshoot is closely related to the yielding of the melt, which occurs because of the shear-induced disentanglement of the constituent polymers. Universal scaling laws have been established in refs 53 and 55 for both the position and the amplitude of the overshoot, and we found that our simulations qualitatively followed the predicted trends.

Furthermore, we found in our simulations that the films needed to be sheared over only relatively short periods of time ($\tau_{shear} \sim 0.1$s for $\dot{\gamma} = 80$ s^{-1}) to achieve well-aligned microdomains. In the experiments, shear was always applied for 1 min or longer, and therefore we surmise that the experimentally measured rheological properties are dominated by their values in the aligned states. We verified this assumption by repeating our shear experiments on prealigned samples, which yielded the same apparent shear viscosity as for the initially unaligned configurations. Hence, we will focus on the flow properties of shear-aligned films, where the cylinders are lying in the *xy*-plane with their axis parallel to the flow direction (*x*). In Figure 8 we plot the shear stress σ_{zx} as a function of applied shear rate $\dot{\gamma}$ for a shear-aligned monolayer of PS−PHMA. This was done to allow for an accurate comparison between the simulations and the experiments, since in the latter we do not have access to $\dot{\gamma}_{eff}$, which takes into account the nonlinear velocity profile across the film (*cf.* Figure 4). Hence, the slope of the curves in Figure 8 corresponds to the *apparent* shear viscosity, which is somewhat smaller than the actual viscosity. The data from the pad shearing experiments and simulations show reasonable agreement (within a factor of ∼2), and we found in both cases the same shear-thinning behavior at intermediate $\dot{\gamma}$.

In order to quantify the asymptotic behavior in the regime $\dot{\gamma} > \dot{\gamma}_{cr}$ we considered the copolymer melt as a power-law fluid and fit our data through

$$\sigma_{zx} = K\dot{\gamma}^n \quad (5)$$

where the flow consistency index K quantifies the viscosity of the fluid, and the dimensionless index n characterizes the type of the fluid ($n < 1$ pseudoplastic; $n = 1$ Newtonian; $n > 1$ dilatant). We determined the exponent in eq 5 to be $n = 0.90$, where the uncertainty was <1% in the simulations and ∼10% in the experiments. This nearly Newtonian response may seem surprising, but in fact a similar nearly Newtonian behavior has previously been reported for cylinder-forming triblock copolymer films in bulk measured *via* capillary rheometry,[56,57] over a comparable range of shear rates. Strong orientation of the cylinder axes in the flow direction is expected in capillary rheometry,[58] so these measurements correspond to the response of the material when sheared along the cylinder axis, exactly as in our present simulations and thin-film experiments.

For the flow consistency index in eq 5 we found $K_{sim} = 500$ Pa·s^n and $K_{exp} = 210$ Pa·s^n (±3% in both cases). This mismatch has several possible origins: in the experiments, slip at the film interface could have lowered the effectively applied shear rate. This hypothesis is corroborated by the fact that the apparent shear viscosity was *lower* in the experiments compared to the simulations, in which we enforced no-slip boundary conditions at the film boundaries. Another reason for the mismatch could stem from the fact that we employed the same time conversion factor retrieved from the PS homopolymer calculations for the PS−PHMA simulations, due to the lack of experimental dynamic data for PHMA and PS−PHMA. This choice is a likely source for error, since PS constitutes only a rather small

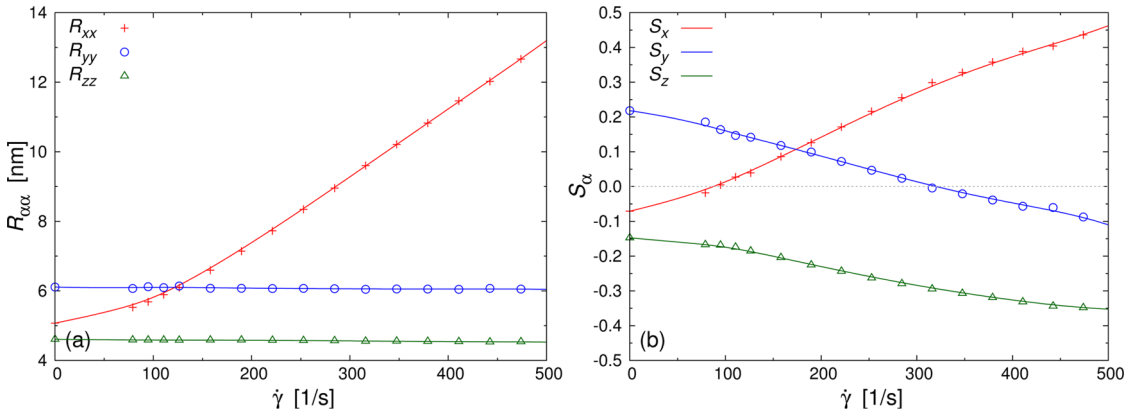

Figure 9. Same as Figure 5 but for a shear-aligned monolayer of PS−PHMA 24/89.

fraction of the entire diblock copolymer, and we expect that self-diffusion in the microphase-separated diblock copolymer melt will be significantly slower than in the homopolymer case. If we assume that shear slip is negligible, we can estimate the time scale for our PS−PHMA simulations by matching the experimental and simulation data shown in Figure 8. Following this procedure, we obtain an alternative time scale of $\tau_{alt} = \tau K_{exp}/K_{sim} \approx 26\ \mu s$, which is, as expected, smaller than the one determined for the PS homopolymer melt ($\tau = 63\ \mu s$). However, we refrained from an *a posteriori* rescaling of our simulation data through τ_{alt}, since we wanted to emphasize the predictive nature of our simulation approach.

In order to better understand the origin of the shear-thinning behavior, we calculated the conformation of the constituent diblock copolymers as the film was sheared. Figure 9 shows the simulation results for both $R_{\alpha\alpha}$ and S_α for a shear-aligned monolayer of PS−PHMA 24/89 as a function of $\dot{\gamma}$, and it is clearly visible that the conformation of the polymers changes drastically due to the applied shear. At rest, the diblocks are aligned and stretched along the *y*-axis due to the formation of cylindrical microdomains along the *x*-axis of the system. Concomitantly, the polymers are slightly squeezed in the *x*-direction and exhibit no significant ordering in this direction. Lastly, it is apparent that the confinement of the melt leads to a compression of the polymers perpendicular to the film surfaces in the *z*-direction. However, the alignment of the polymers changed dramatically as we sheared the films, and we observed a very distinct shear alignment at high $\dot{\gamma}$, similar to the PS homopolymer case (*cf.* Figure 5). In addition, we found that the majority of the alignment takes place in the PHMA matrix block, while the PS block remains almost fully isotropic even at the highest $\dot{\gamma}$ applied (not shown here). This behavior is in stark contrast to previous findings for lamella-forming systems, where the symmetric copolymers were predominantly oriented in the vorticity direction of the flow (*i.e.*, perpendicular to the lamellae) even at very high $\dot{\gamma}$.[59] This fundamental difference stems from the

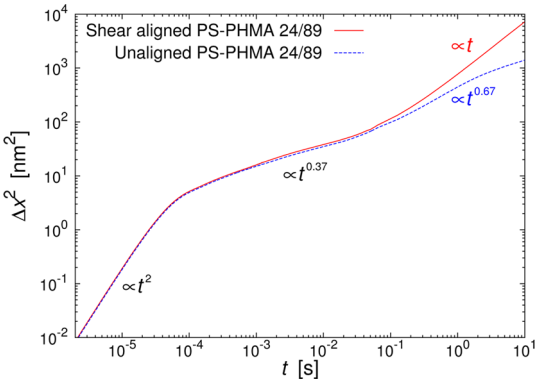

Figure 10. Mean square displacement $\Delta x(t)^2$ for shear-aligned and unaligned monolayers of PS−PHMA 24/89 from simulations.

fact that in the cylinder-forming systems the matrix block can move much more freely, resulting in a significantly lower shear resistance.

Finally, we investigated the contribution of polymer entanglement and microphase separation to the shear viscosity η. To this end, we conducted additional simulations in which we turned off the incompatibility between the two blocks ($\chi = 0$), while keeping all other interactions unchanged. Here, we found the same value for the flow behavior index $n = 0.90$ but a slightly smaller value for the flow consistency index $K_{sim} = 440\ Pa \cdot s^n$. Hence we can conclude that for the shear-aligned films, the main contribution to η stems from the polymer entanglements, and the impact of chemical incompatibility is only minor. The reason for this behavior is that the cylindrical microdomains have already been aligned in flow direction, and the constituent copolymer chains can simply slide along these domains as the film is sheared (see Figure 10). A similar mechanism has been reported for cylinder-forming triblock copolymers in the bulk.[60,61]

However, for unaligned films the situation is entirely different: here, the polymers are highly immobilized and can only move within their proper microdomains due to the large energy barriers associated with the merging of two adjacent domains. In the simulations,

the unaligned films exerted an internal pressure in the *xy*-plane that was ~50 times larger than in the aligned cases. Shear alignment is predominantly driven by the migration of defects through the breakup and reformation of microdomains, and therefore we anticipate the existence of a threshold shear rate $\dot{\gamma}_{thr}$ (and corresponding stress σ_{thr}) below which no alignment can be achieved.[29] We can estimate $\dot{\gamma}_{thr}$ by comparing the advective and diffusive transport rates along the shear direction

$$\dot{\gamma}_{thr} \gtrsim \frac{4D_{x,0}}{HR_{g,0}} \quad (6)$$

where $D_{x,0}$ denotes the diffusion coefficient in the *x*-direction under quiescent conditions, and $R_{g,0}$ and $H\dot{\gamma}_{thr}/4$ are the characteristic length and velocity scales, respectively. In the simulations, we determined $D_{x,0}$ by calculating the mean square displacement $\Delta x(t)^2$ of the individual copolymers and have plotted the results in Figure 10. Here it is apparent that at long times, the unaligned systems exhibit a distinct subdiffusive behavior, while the aligned films show a normal diffusive behavior; in the unaligned case, the copolymers are strongly restricted to the spontaneously formed microdomain they belong to, whereas in the shear aligned films they can explore the whole *x*-range by moving along the cylindrical microdomains. These findings are in line with bulk oscillatory shear experiments of cylinder-forming diblock copolymers, where the elastic modulus G' was significantly greater in the randomly oriented samples than in the shear aligned ones.[62]

We can estimate an upper bound for $\dot{\gamma}_{thr}$ by plugging in the diffusion coefficient for the unaligned case, leading to a value of $\dot{\gamma}_{thr}^{max} \approx 200\ s^{-1}$, which is roughly a factor of 2 larger than the value of $\dot{\gamma}_{thr} = 80\ s^{-1}$ found in the simulations. One possible explanation for this mismatch could be that our estimation neglects the effect of thermal fluctuations, which might effectively lower the barrier for merging two adjacent microdomains and thereby accelerate the restructuring process in the unaligned films. Despite this inaccuracy, we can conclude that eq 6 provides a reasonable order-of-magnitude estimation for $\dot{\gamma}_{thr}$, which can be employed for assessing the feasibility of shear alignment in simulations and experiments.

CONCLUSIONS

In this contribution, we studied the rheological properties of homopolymer and cylinder-forming diblock copolymer thin films under shear by means of experiments and computer simulations. The main focus of the work was the development of a robust theoretical framework that allows for large-scale simulations of specific chemical systems. Such predictive methods are crucial for optimizing and engineering novel synthetic materials, since they allow for significantly faster and more cost-effective prototyping. To demonstrate the feasibility of our approach, we first modeled a PS homopolymer melt and studied its static and dynamic properties. Here, we achieved excellent quantitative agreement with literature experiments on bulk PS: as we sheared the films, we observed a distinct shear-thinning behavior that is strongly related to the disentanglement and alignment of the constituent polymer chains. Furthermore, we were able to predict the onset of this behavior based on the diffusivity at zero shear rate.

In the second part, we studied the flow properties of monolayer films of a cylinder-forming PS–PHMA diblock copolymer, a system of great promise for the fabrication of nanowire arrays used in deep UV polarizers. For these applications, long-range order of the spontaneously self-assembled microdomains is crucial, and we found that such conditions could indeed be achieved through steady shear; the applied shear led to the alignment of the cylindrical microdomains in the flow direction, with the constituent diblock chains oriented perpendicular to the cylinders. Furthermore, we found that the aligned monolayers responded to shear in an almost Newtonian fashion. Lastly, we developed a simple theoretical framework based on equilibrium dynamics data for estimating the minimum shear rate required for ordering the microdomains, and found good agreement between the prediction and simulation result. The details of the alignment process in both simulations and experiments require further investigation, and we plan to study this in a separate publication.

METHODS

Materials. For the homopolymer shear experiments, PS was purchased from Pressure Chemical with M_w = 17.5 kg/mol (Pressure Chemical 41220), 23.75 kg/mol (Pressure Chemical 30811), and 47.5 kg/mol (Pressure Chemical 30908).

The primary diblock copolymer used in this study is cylinder-forming PS–PHMA, which was synthesized *via* sequential living anionic polymerization of styrene (S) and *n*-hexyl methacrylate (HMA). S, HMA, and diphenylethylene (DPE) were purchased from Sigma-Aldrich and degassed prior to use. To remove water and other reactive impurities, S was vacuum transferred from *n*-butyl magnesium, while HMA was vacuum transferred from trioctyl aluminum. Tetrahydrofuran (THF) and methanol were purchased from Fisher and degassed, and *sec*-butyllithium and lithium chloride were purchased from Sigma-Aldrich and used as received. THF was dried over sodium-benzophenone complex for several days prior to use. All of the degassed and cleaned materials were distilled into evacuated flasks immediately prior to polymerizations. The reaction was performed in a glass round-bottom flask under positive N_2 pressure. THF was used as the reaction solvent and cooled to 195 K (using a dry ice-isopropanol bath) prior to monomer addition; the cold temperatures were needed to prevent unwanted side reactions between the living end and the carbonyl group of the HMA. To further prevent side

TABLE 1. Molecular Weight of the Repeat Unit M_0, Molecular Weight of the Kuhn Segment M_K, Entanglement Molecular Weight M_e, Mass Density ρ, and Kuhn Length b of the PS and PHMA Homopolymers[a]

polymer	M_0 [kg/mol]	M_K [kg/mol]	M_e [kg/mol]	ρ [g/cm^3]	b [nm]
PS	0.10415	0.720	19.1	0.969	1.8
PHMA	0.17025	1.62	46.0	0.95	2.44

[a] The properties of PS and PHMA were obtained from refs 40, 41 and refs 41, 65−68, respectively.

reactions, lithium chloride salt was added at 10 equiv relative to initiator prior to the start of the reaction. *Sec*-butyllithium was used to initiate the S block which was allowed to react for 15 min. DPE was then added at 2−3 equiv to reduce the nucleophilicity of the active site, after which a reactor aliquot was taken. Five minutes after the addition of DPE, the HMA monomer was charged at an approximate rate of 2 mL/min. The reaction proceeded for 30 min and was then terminated with methanol. The reaction contained a small amount of terminated PS block, which was removed by liquid−liquid fractionation using toluene (solvent) and acetonitrile (nonsolvent).

The composition of the block copolymer was determined using ^{1}HNMR spectroscopy in $CDCl_3$ on a 500 MHz Bruker AVANCE by comparing the peak areas of the PS aromatic protons and PHMA methylene protons. The dispersity, Đ, and molecular weight, M, were determined by size exclusion chromotagraphy (SEC; Waters 515 HPLC pump, two 30 cm Agilent PLgel Mixed-C columns, and Wyatt Optilab T-rEX differential refractometer) in THF at 308 K. The column elution times were calibrated with a series of narrow-distribution PS standards of known molecular weight, allowing for absolute molecular weight determination of the PS block. The absolute molecular weight of the diblock was then determined using the PS block molecular weight coupled with the composition measured by NMR, yielding number-average molecular weights $M_{n,PS}$ = 24 kg/mol and $M_{n,PHMA}$ = 89 kg/mol. The diblock dispersity was measured to be Đ = 1.10.

Thin films were prepared by dissolving polymer in toluene (purchased from VWR, used as received) and spin-coating onto silicon wafers (with native oxide). The wafers were purchased from Silicon Quest and liberally washed with toluene prior to use. Polymer film thickness was determined using a Gaertner Scientific LS116S300 ellipsometer (λ = 632.8 nm). We observed that the PHMA (matrix) block wets both the substrate and the surface exposed to the polydimethylsiloxane (PDMS) pad.

Table 1 lists the relevant physical information for the constituent monomers. From this we determined the degree of polymerization, N = 753, and the volume fraction of the PS minority block, $f \approx 0.21$. We calculated the end-to-end distance of the copolymer in the melt, R_e, using the freely jointed chain model as $R_e^2 = \sum_i^{N-1} b_i^2$ = 20.8 nm.[40] We estimated 3.2 entanglements per copolymer chain based on the entanglement molecular weights, M_e, of the two blocks. Furthermore, we determined the interdigitation number, which is a measure for the strength of fluctuations,[63] as $\bar{N} = \rho R_e^3/N$ = 46.1. The Flory−Huggins parameter is given by $\chi \approx 0.035 + 3.93\ \mathrm{K}/T$,[64] which is valid for 423 K < T < 488 K. Both experiments and simulations have been conducted at T = 458 K, yielding a value of $\chi \approx 0.044$ (χN = 32.8).

Pad Shearing. The wafer-supported films were placed onto a hot plate at the desired temperature. We prepared a smooth cross-linked PDMS pad (∼1 mm thick) by mixing Dow Corning Sylgard 184 at a weight ratio of ∼1:15 curing agent to elastomer and curing it for 2 h at $T \approx$ 333 K. We then trimmed the pad to a prescribed size (typically 1 cm × 1 cm), placed it in contact with the film, and allowed it to equilibrate for 10 min. We then sheared the film by imparting a constant lateral force to the pad,[9] while at the same time applying a normal force (typically ∼1 kg) to minimize slip between the pad and polymer film. After some time (typically between 1 min and several hours) the shear stress is removed and the translation of the pad (∼1−10 mm) is measured using an optical microscope with a stage capable of ±10 μm lateral movement. The apparent shear rate was then computed using the distance of translation, the film thickness, and the time of applied shear.

We validated this method by measuring the shear viscosity of three reference samples of PS homopolymers with weight-average molecular weights M_w = 17.5, 23.8, and 47.5 kg/mol. The film thickness was H = 100 nm and the applied shear was well below the onset of shear-thinning in all cases. We measured zero-shear viscosities of η_0 = 105, 242, and 3443 Pa·s (each ∼ ± 15%), which are in very good agreement with the literature values of η_0 = 105, 313, and 3725 Pa·s.[44] Thus, we can conclude that the applied pad shearing method can be employed for measuring the (apparent) shear viscosity of thin polymer melts.

Simulation Model. We utilize the recently developed TICG model[30] for simulating the polymer melts, which preserves the relevant system properties, such as chain connectivity, microphase separation and finite compressibility of the melt. In this model, each diblock copolymer is discretized into a linear chain with N spherical beads with diameter a and unit mass m. In what follows, we will denote their positions and velocities as $\mathbf{r}_i$ and $\mathbf{v}_i$, respectively, and refer to the different particle types simply as A or B for the sake of generality. The chemical bonds between two adjacent beads i and j are described by Hookean springs:

$$\frac{U_b(r_{ij})}{k_B T} = \frac{3}{2}\left(\frac{r_{ij}}{b_i}\right)^2 \tag{7}$$

where k_B denotes the Boltzmann constant, T the temperature, r_{ij} the interparticle distance, and b_i the (equilibrium) bond length of the connecting spring. The monomer−monomer interaction U_{mm} between two beads i and j is governed by[30]

$$\frac{U_{mm}(r_{ij})}{k_B T} = \frac{\sqrt{\bar{N}}}{R_e^3}\left[\kappa N + \chi N(1-\delta_{ij})\right]\int_V \omega(\mathbf{r}-\mathbf{r_i})\omega(\mathbf{r}-\mathbf{r_j})\,\mathrm{d}\mathbf{r} \tag{8}$$

Here, the compressibility of the melt is set through the parameter κ, while the incompatibility of the type A and B monomers is quantified by the Flory−Huggins parameter χ. Lastly, $\omega(\mathbf{r})$ denotes the density cloud around each particle's center, where we chose spherical steplike functions with $\omega(r) = 1$ for $r < a/2$ and $\omega(r) = 0$ elsewhere.

Table 1 shows the relevant properties of the constituent homopolymers from the experimental literature, which we then used to determine the characteristics of the PS−PHMA 24/89 diblock copolymer chains (see Materials). Subsequently, we mapped each polymer to a linear chain with N = 32 beads, while keeping the parameters f and $\bar{N}$ fixed during the mapping procedure. We chose κN = 15 for the compressibility term in U_{mm} and a number density of $\rho = 4.5\ a^{-3}$ according to the arguments brought forward in refs 30 and 35. Furthermore, we set the bond lengths between two consecutive A and B beads to $b_A = a$ and $b_B = 1.4\ a$ respectively, thereby preserving the experimental ratio between the Kuhn lengths b_{HMA}/b_S = 1.4. Maintaining this ratio is crucial, since the difference in bond rigidity has a significant impact on the wetting behavior of the block copolymer in thin films.[38,69] From these data, we get the conversion factor $a \approx$ 3.2 nm for the PS 75 homopolymer, and $a \approx$ 2.9 nm for the PS−PHMA 24/89 diblock copolymer.

In addition to these intra- and intermolecular forces, we have to specify the surface-bead interactions due to the confined nature of the system. In our setup, we applied periodic boundary conditions in the x and y direction, and placed two impenetrable walls at $z = \pm (H + a)/2$, which interact with the beads *via*

$$\frac{U_{wall}(z)}{k_B T} = \varepsilon_{S,i}\left(\frac{z}{a}\right)^{-6} \tag{9}$$

where z denotes the shortest distance to each wall and the strength of the repulsion can be controlled through the parameter $\varepsilon_{S,i}$. In order to mimic the experimental wetting characteristics, we set $\varepsilon_{S,A} = 6\ k_B T$ and $\varepsilon_{S,B} = 2\ k_B T$ for the minority and majority block, respectively.[36]

We employed the standard velocity Verlet algorithm[70,71] with a time step of $\Delta t = 0.03$ in conjunction with a DPD thermostat[31−34] for calculating the particle trajectories. The DPD model consists of the summation of conservative forces ($\mathbf{F}_c = -\nabla U$), random noise ($\mathbf{F}_r$), and dissipative forces ($\mathbf{F}_d$). The latter two are given by

$$\mathbf{F}_r(r_{ij}) = -\lambda\sqrt{\frac{6\xi k_B T}{\Delta t}}\,\omega_d(r_{ij})\hat{\mathbf{r}}_{ij} \quad (10)$$

$$\mathbf{F}_d(r_{ij}) = -\xi\omega_d^2(r_{ij})(\mathbf{v}_{ij}\cdot\mathbf{r}_{ij})\hat{\mathbf{r}}_{ij} \quad (11)$$

where λ denotes a uniformly distributed random number in the range $[-1,+1]$, $\xi = 3(mk_BT)^{1/2}/a$ is the molecular friction coefficient, $\hat{\mathbf{r}}_{ij}$ the unit vector between particles i and j, and $\mathbf{v}_{ij} = \mathbf{v}_i - \mathbf{v}_j$. Furthermore, we chose the weight function as $\omega_d(r_{ij}) = 1 - r_{ij}/a$ for $r_{ij} < a$, and 0 otherwise. Shear flow has been implemented by implicitly moving the upper and lower walls (see SI for more details).

Because of the ultrasoft nature of the monomer−monomer interactions, bond crossings are not prevented by excluded volume effects, resulting in artificially accelerated dynamics and unrealistic rheological properties. In order to recover the appropriate topological constraints and reptation dynamics in the melt, we include virtual slip-springs.[37,39] Here, we employed the multichain approach developed in ref 39, where chain beads are temporarily cross-linked *via* Hookean springs. These springs can move along the chains in discrete steps from bead to bead, and may also relocate from one chain end to another. The movement of these slip-springs is governed by a Metropolis Monte Carlo (MC) algorithm, and we repeatedly alternate between the DPD and MC sequences (500 steps each) to compute the dynamics of the polymers and slip-springs, respectively. Here, we chose a slip-spring density of 0.1 ρ and set their stiffness to $k = 2\,k_BT/a^2$ for both the homopolymer and diblock copolymer case. This choice corresponds to an average of 3.2 slip-springs per chain, which is the same number as expected for experimental PS−PHMA 24/89 and slightly less than the value of 3.9 expected for PS 75. We used the HOOMD package[72−74] for the DPD portion, and ran each shear simulation for a total of 1.5×10^6 DPD steps (plus the same number of MC steps).

Conflict of Interest: The authors declare no competing financial interest.

Acknowledgment. The authors would like to thank Juan J. de Pablo for helpful discussions. This work has been supported by the Princeton Center for Complex Materials (PCCM), a U.S. National Science Foundation Materials Research Science and Engineering Center (Grant DMR-0819860).

Supporting Information Available: Detailed description of the shear method employed in the simulations. This material is available free of charge *via* the Internet at http://pubs.acs.org.

REFERENCES AND NOTES

1. Stoykovich, M. P.; Kang, H.; Doulas, K. C.; Liu, G.; Liu, C.-C.; de Pablo, J. J.; Müller, M.; Nealey, P. F. Directed Self-Assembly of Block Copolymers for Nanolithography: Fabrication of Isolated Features and Essential Integrated Circuit Geometries. *ACS Nano* **2007**, *1*, 168–175.
2. Ruiz, R.; Kang, H. M.; Detcheverry, F. A.; Dobisz, E.; Kercher, D. S.; Albrecht, T. R.; de Pablo, J. J.; Nealey, P. F. Density Multiplication and Improved Lithography by Directed Block Copolymer Assembly. *Science* **2008**, *321*, 936–939.
3. Marencic, A. P.; Register, R. A. Controlling Order in Block Copolymer Thin Films for Nanopatterning Applications. *Annu. Rev. Chem. Biomol. Eng.* **2010**, *1*, 277–297.
4. Matsen, M. W.; Bates, F. S. Unifying Weak- and Strong-Segregation Block Copolymer Theories. *Macromolecules* **1996**, *29*, 1091–1098.
5. Pelletier, V.; Asakawa, K.; Wu, M.; Adamson, D. H.; Register, R. A.; Chaikin, P. M. Aluminum Nanowire Polarizing Grids: Fabrication and Analysis. *Appl. Phys. Lett.* **2006**, *88*, 211114.
6. Hong, Y.-R.; Asakawa, K.; Adamson, D. H.; Chaikin, P. M.; Register, R. A. Silicon Nanowire Grid Polarizer for Very Deep Ultraviolet Fabricated from a Shear-Aligned Diblock Copolymer Template. *Opt. Lett.* **2007**, *32*, 3125–3127.
7. Papalia, J. M.; Adamson, D. H.; Chaikin, P. M.; Register, R. A. Silicon Nanowire Polarizers for Far Ultraviolet (sub-200 nm) Applications: Modeling and Fabrication. *J. Appl. Phys.* **2010**, *107*, 084305.
8. Kim, S. Y.; Gwyther, J.; Manners, I.; Chaikin, P. M.; Register, R. A. Metal-Containing Block Copolymer Thin Films Yield Wire Grid Polarizers with High Aspect Ratio. *Adv. Mater.* **2013**, *26*, 791–795.
9. Angelescu, D. E.; Waller, J. H.; Adamson, D. H.; Deshpande, P.; Chou, S. Y.; Register, R. A.; Chaikin, P. M. Macroscopic Orientation of Block Copolymer Cylinders in Single-Layer Films by Shearing. *Adv. Mater.* **2004**, *16*, 1736–1740.
10. Singh, G.; Yager, K. G.; Berry, B.; Kim, H.-C.; Karim, A. Dynamic Thermal Field-Induced Gradient Soft-Shear for Highly Oriented Block Copolymer Thin Films. *ACS Nano* **2012**, *6*, 10335–10342.
11. Amundson, K.; Helfand, E.; Quan, X.; Smith, S. D. Alignment of Lamellar Block Copolymer Microstructure in an Electric Field. 1. Alignment Kinetics. *Macromolecules* **1993**, *26*, 2698–2703.
12. Amundson, K.; Helfand, E.; Quan, X.; Hudson, S. D.; Smith, S. D. Alignment of Lamellar Block Copolymer Microstructure in an Electric Field. 2. Mechanisms of Alignment. *Macromolecules* **1994**, *27*, 6559–6570.
13. Mansky, P.; DeRouchey, J.; Russell, T. P.; Mays, J.; Pitsikalis, M.; Morkved, T.; Jaeger, H. Large-Area Domain Alignment in Block Copolymer Thin Films Using Electric Fields. *Macromolecules* **1998**, *31*, 4399–4401.
14. Pickett, G. T. Lateral Copolymer Domain Patterning through Thermal Gradients. *J. Chem. Phys.* **2002**, *116*, 2692–2695.
15. Berry, B. C.; Bosse, A. W.; Douglas, J. F.; Jones, R. L.; Karim, A. Orientational Order in Block Copolymer Films Zone Annealed below the Order-Disorder Transition Temperature. *Nano Lett.* **2007**, *7*, 2789–2794.
16. Yager, K. G.; Fredin, X.; Zhang, N. J.; Berry, B. C.; Karim, A.; Jones, R. L. Evolution of Block-Copolymer Order through a Moving Thermal Zone. *Soft Matter* **2010**, *6*, 92–99.
17. Angelescu, D. E.; Waller, J. H.; Register, R. A.; Chaikin, P. M. Shear-Induced Alignment in Thin Films of Spherical Nanodomains. *Adv. Mater.* **2005**, *17*, 1878–1881.
18. Pujari, S.; Keaton, M. A.; Chaikin, P. M.; Register, R. A. Alignment of Perpendicular Lamellae in Block Copolymer Thin Films by Shearing. *Soft Matter* **2012**, *8*, 5358–5363.
19. Angelescu, D. E.; Waller, J. H.; Wu, M. W.; Chaikin, P. M.; Register, R. A. Method and Apparatus for Providing Shear-Induced Alignment of Nanostructure in Thin Films. US patent application 11/011,495, 2006.
20. Singh, G.; Batra, S.; Zhang, R.; Yuan, H.; Yager, K. G.; Cakmak, M.; Berry, B.; Karim, A. Large-Scale Roll-to-Roll Fabrication of Vertically Oriented Block Copolymer Thin Films. *ACS Nano* **2013**, *7*, 5291–5299.
21. Müller-Plathe, F. Coarse-Graining in Polymer Simulation: From the Atomistic to the Mesoscopic Scale and Back. *ChemPhysChem* **2002**, *3*, 754–769.
22. Rychkov, I. Block Copolymers Under Shear Flow. *Macromol. Theory Simul.* **2005**, *14*, 207–242.
23. Pinna, M.; Zvelindovsky, V. Large Scale Simulation of Block Copolymers with Cell Dynamics. *Eur. Phys. J. B* **2012**, *85*, 210.
24. Karimi-Varzaneh, H. A.; van der Vegt, N. F. A.; Müller-Plathe, F.; Carbone, P. How Good Are Coarse-Grained Polymer Models? A Comparison for Atactic Polystyrene. *ChemPhysChem* **2012**, *13*, 3428–3439.
25. Nikoubashman, A.; Register, R. A.; Panagiotopoulos, A. Z. Simulations of Shear-Induced Transitions in Block Copolymer Thin Films. *Soft Matter* **2013**, *9*, 9960–9971.
26. Harmandaris, V. A.; Adhikari, N. P.; van der Vegt, N. F. A.; Kremer, K. Hierarchical Modeling of Polystyrene: From Atomistic to Coarse-Grained Simulations. *Macromolecules* **2006**, *39*, 6708–6719.

27. Rossi, G.; Monticelli, L.; Puisto, S. R.; Vattulainen, I.; Ala-Nissila, T. Coarse-Graining Polymers with the MARTINI Force-Field: Polystyrene as a Benchmark Case. *Soft Matter* **2011**, *7*, 698–708.
28. Matsen, M. W.; Schick, M. Stable and Unstable Phases of a Diblock Copolymer Melt. *Phys. Rev. Lett.* **1994**, *72*, 2660–2663.
29. Ren, S. R.; Hamley, I. W.; Teixeira, P. I. C.; Olmsted, P. D. Cell Dynamics Simulations of Shear-Induced Alignment and Defect Annihilation in Stripe Patterns Formed by Block Copolymers. *Phys. Rev. E: Stat., Nonlinear, Soft Matter Phys.* **2001**, *63*, 041503.
30. Pike, D. Q.; Detcheverry, F. A.; Müller, M.; de Pablo, J. J. Theoretically Informed Coarse Grain Simulations of Polymeric Systems. *J. Chem. Phys.* **2009**, *131*, 084903.
31. Hoogerbrugge, P. J.; Koelman, J. M. V. A. Simulating Microscopic Hydrodynamic Phenomena with Dissipative Particle Dynamics. *Europhys. Lett.* **1992**, *19*, 155–160.
32. Koelman, J. M. V. A.; Hoogerbrugge, P. J. Dynamic Simulations of Hard-Sphere Suspensions Under Steady Shear. *Europhys. Lett.* **1993**, *21*, 363–368.
33. Español, P.; Warren, P. B. Statistical Mechanics of Dissipative Particle Dynamics. *Europhys. Lett.* **1995**, *30*, 191–196.
34. Groot, R. D.; Warren, P. B. Dissipative Particle Dynamics: Bridging the Gap between Atomistic and Mesoscopic Simulation. *J. Chem. Phys.* **1997**, *107*, 4423–4435.
35. Peters, B. L.; Ramírez-Hernández, A.; Pike, D. Q.; Müller, M.; de Pablo, J. J. Nonequilibrium Simulations of Lamellae Forming Block Copolymers under Steady Shear: A Comparison of Dissipative Particle Dynamics and Brownian Dynamics. *Macromolecules* **2012**, *45*, 8109–8116.
36. Nikoubashman, A.; Register, R. A.; Panagiotopoulos, A. Z. Self-Assembly of Cylinder-Forming Diblock Copolymer Thin Films. *Macromolecules* **2013**, *46*, 6651–6658.
37. Ramírez-Hernández, A.; Detcheverry, F. A.; Peters, B. L.; Chappa, V. C.; Schweizer, K. S.; Müller, M.; de Pablo, J. J. Dynamical Simulations of Coarse Grain Polymeric Systems: Rouse and Entangled Dynamics. *Macromolecules* **2013**, *46*, 6287–6299.
38. Nikoubashman, A.; Register, R. A.; Panagiotopoulos, A. Z. Sequential Domain Realignment Driven by Conformational Asymmetry in Block Copolymer Thin Films. *Macromolecules* **2014**, *47*, 1193–1198.
39. Langeloth, M.; Masubuchi, Y.; Böhm, M. C.; Müller-Plathe, F. Recovering the Reptation Dynamics of Polymer Melts in Dissipative Particle Dynamics Simulations *via* Slip-Springs. *J. Chem. Phys.* **2013**, *138*, 104907.
40. Rubinstein, M.; Colby, R. H. *Polymer Physics*; Oxford University Press: Oxford, 2003.
41. Fetters, L. J.; Lohse, D. J.; Colby, R. H. In *Physical Properties of Polymers Handbook*, 2nd ed.; Mark, J. E., Ed.; Springer: New York, 2007; pp 447−454.
42. Antonietti, M.; Fölsch, K. J.; Sillescu, H. Critical Chain Lengths in Polystyrene Bulk Diffusion. *Makromol. Chem.* **1987**, *188*, 2317–2324.
43. Likhtman, A. E. *Viscoelasticity and Molecular Rheology*; Elsevier: Amsterdam, 2012; Vol. 1; pp 133−179.
44. McKenna, G. B.; Hadziioannou, G.; Lutz, P.; Hild, G.; Strazielle, C.; Straupe, C.; Rempp, P.; Kovacs, A. J. Dilute Solution Characterization of Cyclic Polystyrene Molecules and Their Zero-Shear Viscosity in the Melt. *Macromolecules* **1987**, *20*, 498–512.
45. Hieber, C. A.; Chiang, H. H. Some Correlations Involving the Shear Viscosity of Polystyrene Melts. *Rheol. Acta* **1989**, *28*, 321–332.
46. Carreau, P. J. Rheological Equations from Molecular Network Theories. *Trans. Soc. Rheol.* **1972**, *16*, 99–127.
47. Verband Deutscher Maschinen und Anlagenbau. *Rheologie*; Carl Hanser Verlag: Munich, 1982.
48. Kühnle, H. Evaluation of the Viscoelastic Temperature and Pressure Shift Factor Over the Full Range of Shear Rates. *Int. Polym. Proc.* **1987**, *1*, 89–97.
49. Doi, M.; Edwards, S. F. *The Theory of Polymer Dynamics*; Clarendon Press: Oxford, 1999.
50. Rogers, S. S.; Mandelkern, L. Glass Transitions of the Poly(*n*-Alkyl Methacrylates). *J. Phys. Chem.* **1957**, *61*, 985–991.
51. Huppler, J. D.; MacDonald, I. F.; Ashare, E.; Spriggs, T. W.; Bird, R. B.; Holmes, L. A. Rheological Properties of Three Solutions. Part II. Relaxation and Growth of Shear and Normal Stresses. *Trans. Soc. Rheol.* **1967**, *11*, 181–204.
52. Crawley, R. L.; Graessley, W. W. Geometry Effects on Stress Transient Data Obtained by Cone and Plate Flow. *Trans. Soc. Rheol.* **1977**, *21*, 19–49.
53. Ravindranath, S.; Wang, S.-Q. Universal Scaling Characteristics of Stress Overshoot in Startup Shear of Entangled Polymer Solutions. *J. Rheol.* **2008**, *52*, 681–695.
54. Wang, Y.; Wang, S.-Q. Exploring Stress Overshoot Phenomenon Upon Startup Deformation of Entangled Linear Polymeric Liquids. *J. Rheol.* **2009**, *53*, 1389–1401.
55. Snijkers, F.; Vlassopoulos, D. Cone-Partitioned-Plate Geometry for the ARES Rheometer with Temperature Control. *J. Rheol.* **2011**, *55*, 1167–1186.
56. Ghijsels, A.; Raadsen, J. A Collaborative Study on the Melt Rheology of a Styrene-Butadiene-Styrene Block Copolymer. *Pure Appl. Chem.* **1980**, *52*, 1359–1386.
57. Han, J.; Feng, D.; Choi-Feng, C.; Han, C. D. Effects of Sample Preparation and Flow Geometry on the Rheological Behaviour and Morphology of Microphase-Separated Block Copolymers: Comparison of Cone-and-Plate and Capillary Data. *Polymer* **1995**, *36*, 155–167.
58. Folkes, M. J.; Keller, A.; Scalisi, F. P. An Extrusion Technique for the Preparation of "Single Crystals" of Block Copolymers. *Kolloid Z. Z. Polym.* **1973**, *251*, 1–4.
59. Chremos, A.; Chaikin, P. M.; Register, R. A.; Panagiotopoulos, A. Z. Shear-Induced Alignment of Lamellae in Thin Films of Diblock Copolymers. *Soft Matter* **2012**, *8*, 7803–7811.
60. Ryu, C. Y.; Lee, M. S.; Hajduk, D. A.; Lodge, T. P. Structure and Viscoelasticity of Matched Asymmetric Diblock and Triblock Copolymers in the Cylinder and Sphere Microstructures. *J. Polym. Sci., Part B: Polym. Phys.* **1997**, *35*, 2811–2823.
61. Daniel, C.; Hamley, I. W. Extensional and Shear Rheometry of Oriented Triblock Copolymers. *Rheol. Acta* **2000**, *39*, 191–200.
62. Almdal, K.; Bates, F. S.; Mortensen, K. Order, Disorder, and Fluctuation Effects in an Asymmetric Poly(Ethylene-Propylene)-Poly(Ethylethylene) Diblock Copolymer. *J. Chem. Phys.* **1992**, *96*, 9122–9132.
63. Daoulas, K.; Müller, M.; de Pablo, J. J.; Nealey, P. F.; Smith, G. Morphology of Multi-Component Polymer Systems: Single Chain in Mean Field Simulation Studies. *Soft Matter* **2006**, *2*, 573–583.
64. Ruzette, A. V. G.; Banerjee, P.; Mayes, A. M.; Pollard, M.; Russell, T. P.; Jerome, R.; Slawecki, T.; Hjelm, R.; Thiyagarajan, P. Phase Behavior of Diblock Copolymers between Styrene and *n*-Alkyl Methacrylates. *Macromolecules* **1998**, *31*, 8509–8516.
65. Ferry, J. D.; Child, W. C., Jr. Dynamic Mechanical Properties of Poly-*n*-Hexyl Methacrylate. *J. Colloid Sci.* **1957**, *12*, 389–399.
66. Chinai, S. N. Poly-*n*-Hexyl Methacrylate. IV. Dilute Solution Properties by Viscosity and Light Scattering. *J. Polym. Sci., Part A: Polym. Chem.* **1957**, *25*, 413–427.
67. Aharoni, S. M. Correlations between Chain Parameters and the Plateau Modulus of Polymers. *Macromolecules* **1986**, *19*, 426–434.
68. Mays, J. W.; Hadjichristidis, N. Characteristic Ratios of Polymethacrylates. *J. Macromol. Sci., Rev. Macromol. Chem. Phys.* **1988**, *28*, 371–401.
69. Kellogg, G. J.; Walton, D. G.; Mayes, A. M.; Lambooy, P.; Russell, T. P.; Gallagher, P. D.; Satija, S. K. Observed Surface Energy Effects in Confined Diblock Copolymers. *Phys. Rev. Lett.* **1996**, *76*, 2503–2506.
70. Allen, M. P.; Tildesley, D. J. In *Computer Simulation of Liquids*; Allen, M. P., Tildesley, D. J., Eds.; Oxford University Press: Oxford, 1989.
71. Frenkel, D.; Smit, B. In *Understanding Molecular Simulation: From Algorithms to Applications*; Frenkel, D., Smit, B., Eds.; Academic Press: Waltham, MA, 2001.

72. *HOOMD-blue*; University of Michigan: Ann Arbor, MI, 2014; http://codeblue.umich.edu/hoomd-blue.
73. Anderson, J. A.; Lorenz, C. D.; Travesset, A. General Purpose Molecular Dynamics Simulations Fully Implemented on Graphics Processing Units. *J. Comput. Phys.* **2008**, *227*, 5342–5359.
74. Phillips, C. L.; Anderson, J. A.; Glotzer, S. C. Pseudo-Random Number Generation for Brownian Dynamics and Dissipative Particle Dynamics Simulations on GPU Devices. *J. Comput. Phys.* **2011**, *230*, 7191–7201.